Inorg. Chem. **2008**, *47*, 2562−2568

Four Isomorphous Phosphates $AM_3P_4O_{14}$ (A = Sr, Ba; M = Co, Mn) with Antiferromagnetic−Antiferromagnetic−Ferromagnetic Trimerized Chains, Showing 1/3 Quantum Magnetization Plateaus Only in the Manganese(II) System

Tao Yang,[†] Yan Zhang,[‡] Sihai Yang,[†] Guobao Li,[†] Ming Xiong,[§] Fuhui Liao,[†] and Jianhua Lin*,[†]

Beijing National Laboratory for Molecular Sciences, State Key Laboratory of Rare Earth Materials Chemistry and Applications, College of Chemistry and Molecular Engineering, Peking University, Beijing 100871, People's Republic of China, Department of Physics, Peking University, 100871, People's Republic of China, and X-ray Laboratory, China University of Geoscience, Beijing, 100083, People's Republic of China

Received September 25, 2007

The four new phosphates $BaCo_3P_4O_{14}$ (**1**), $SrCo_3P_4O_{14}$ (**2**), $BaMn_3P_4O_{14}$ (**3**), and $SrMn_3P_4O_{14}$ (**4**) were hydrothermally synthesized and characterized structurally and magnetically. They are isostructural with $ANi_3P_4O_{14}$ (A = Ca, Sr, Pb, Ba), crystallizing in the monoclinic space group $P2_1/c$. The CoO_6 (or MnO_6) octahedra share edges to from zigzag chains along the *b* axis, which are further interconnected by P_2O_7 groups into a three-dimensional structure. Preliminary magnetic measurements on powder samples indicate that **1**, **2**, and **4** are spin-canted antiferromagnets and **3** is a pure antiferromagnet at low field; long-range orderings were established respectively at $T_{critical} \approx 8.2$ K for **1**, 6.5 K for **2**, and 2.6 K for both **3** and **4**; field-induced spin-flop-like transitions occur respectively at $H_c \approx 25$ kOe for **1**, 4 kOe for **2**, 3 kOe for **3**, and 0.7 kOe for **4.** Interestingly, together with the known Ni analogues, they all apply the same antiferromagnetic−antiferromagnetic−ferromagnetic (AAF) trimerized chain model, whereas the 1/3 quantum magnetization plateau only appears in the Mn system. By qualitative analysis, we conclude that the appearance of quantum magnetization plateaus in the AAF chain compounds requires both good 1D characteristics and strong AF intrachain interactions.

Introduction

Phosphates have attracted considerable attention in the past few years as a promising family of functional materials, particularly after the discovery of microporous aluminophosphates in 1982, designated $AlPO_4$-n.[1] In metal phosphates, phosphorus atoms are tetrahedrally coordinated, while the metal ions can be coordinated in tetrahedral, pyramidal, or octahedral environments; thus, the structures of metal phosphates are generally complex, and these compounds may form diverse materials and exhibit various interesting functional properties, such as nonlinear optical properties ($KTiOPO_4$, for example),[2] ionic conductivity (NASICON family[3] and Li_xFePO_4[4]), and also magnetic properties if transition-metal ions are incorporated. In the quasi-ternary A−M−P−O systems (A = alkaline-earth metal and M = transition metal), several phosphates have been structurally and/or magnetically characterized, including $AM_2(PO_4)_2$ (A

* To whom correspondence should be addressed. E-mail: jhlin@pku.edu.cn. Tel: (8610)62751715. Fax: (8610)62751708.
[†] College of Chemistry and Molecular Engineering, Peking University.
[‡] Department of Physics, Peking University.
[§] China University of Geoscience.

(1) Wilson, S. T.; Loc, B. M.; Messina, C. A.; Cannan, T. R.; Flanigen, E. M. *J. Am. Chem. Soc.* **1982**, *104*, 1146–1147.
(2) (a) Bierlein, J. D.; Vanherzeele, H. J. *Opt. Soc. Am. B: Opt. Phys.* **1989**, *6*, 622. (b) Vanherzeele, H. *Appl. Opt.* **1988**, *27*, 3608.
(3) (a) Rodrigo, J. L.; Carrasco, P.; Alamo, J. *Mater. Res. Bull.* **1989**, *24*, 611–618. (b) Alami Talbi, M.; Brochu, R.; Parent, C.; Rabardel, L.; Le Flem, G. *J. Solid State Chem.* **1994**, *110*, 350–355. (c) Arbi, K.; Lazarraga, M. G.; Chehimi, D. B.; Ayadi-Trabelsi, M.; Rojo, J. M.; Sanz, J. *Chem. Mater.* **2004**, *16*, 255–262. (d) Patoux, S.; Rousse, G.; Leriche, J. B.; Masquelier, C. *Chem. Mater.* **2003**, *15*, 2084–2093. (e) Maldonado-Manso, P.; Losilla, E. R.; Martinez-Lara, M.; Aranda, M. A. G.; Bruque, S.; Mouahid, F. E.; Zahir, M. *Chem. Mater.* **2003**, *15*, 1879–1885.
(4) Ellis, B.; Perry, L. K.; Ryan, D. H.; Nazar, L. F. *J. Am. Chem. Soc.* **2006**, *128*, 11416–11422.
(5) Moqine, A.; Boukhari, A.; Darriet, J. *J. Solid State Chem.* **1993**, *107*, 362–367.

10.1021/ic702346e CCC: $40.75

Published on Web 03/12/2008

= Ca, Sr, Ba, Pb; M = Mg and transition metals),[5–14] AMP_2O_7 (A = Ca, Sr, Ba, Pb and M = Cu, Co, Ni),[15–21] $A_2M(PO_4)_2$ (A = Sr, Ba and M = Cu, Co, Ni),[22–24] $A_3Cu_3(PO_4)_4$ (A = Ca, Sr, Pb)[25,26] and $AM_3P_4O_{14}$ (A = Ca, M = Fe, Co; A = Ca, Sr, Ba, Pb, M = Ni).[27,28] In particular, the copper phosphates have been extensively studied, due to their low-dimensional quantum magnetism.[29] For example, $M_2Cu(PO_4)_2$ (M = Ba, Sr)[22,24] and $ACuP_2O_7$ (A = Sr, Pb, Ba)[16,20] behave as typical 1D uniform $S = 1/2$ Heisenberg antiferromagnetic chains, $ACu_2(PO_4)_2$ (A = Sr, Pb) shows linear antiferromagnetic interactions and has a spin gap above the spin-singlet ground state, which leads to a 1/2 magnetization plateau observed between 50 and 63 T at 1.3 K for $SrCu_2(PO_4)_2$,[13,14] and $A_3Cu_3(PO_4)_4$ (A = Ca, Sr, Pb) has ferrimagnetic trimer clusters ($S_{total} = 1/2$) and shows 1/3 quantum magnetization plateaus.[25,26]

On the other hand, the study of quantum spin systems, in particular the one-dimensional models, has been one of the main subjects of condensed matter physics stimulated by Haldane's conjecture: an energy gap exists for the Heisenberg antiferromagnetic chain with integer spin values, while there is no gap for the chain with half-integer spins.[30] This Haldane gap was then experimentally proved in the $S = 1$ compound $Ni(C_2H_8N_2)_2NO_2(ClO_4)$.[31] In addition, another quantum mechanism derived phenomenon called magnetization plateaus was also studied both theoretically and experimentally. One important result is that magnetization curves at 0 K in Heisenberg antiferromagnetic bond-altering chains might have plateaus at m that satisfies the formula of $n(S - m) =$ integer.[32] Here, n is the period of the ground state and S and m respectively represent the total spin and magnetization per unit cell. Actually, this is a necessary condition and whether the plateau exists or not depends on the details of the model.[33] To date, only a few homometallic chain compounds such as $[Ni_2(Medpt)_2(\mu\text{-ox})(\mu\text{-}N_3)ClO_4 \cdot 0.5H_2O$, $[Ni_2(dpt)_2(\mu\text{-ox})(\mu\text{-}N_3)](PF_6)$, $[Ni(333\text{-tet})(\mu\text{-}NO_2)]ClO_4$, and $Cu_3(P_2O_6OH)_2$ have 1/2 or 1/3 quantum magnetization plateaus.[34]

For ferromagnetic−antiferromagnetic mixed chains, numerical calculations were performed in theory using a ferromagnetic−ferromagnetic−antiferromagnetic (FFA) trimer model, which predicted that the magnetization plateau can only be observed when the J_F/J_{AF} ratios are small.[35] Experimentally, a 1/3 magnetization plateau was found in a FFAA tetramer chain compound, $Cu(3\text{-}Clpy)_2(N_3)_2$;[36] a 1/2 plateau was observed in the alternating $S = 1$ and $S = 0$ dimer chain compound $(CH_3)_2NH_2CuCl_3$.[37] Recently, the nickel phosphates $ANi_3P_4O_{14}$ (A = Ca, Sr, Pb, Ba),[28] consisting of edge-sharing MO_6 zigzag chains, were declared to be the first observation of ferrimagnetic long-range ordering caused by the periodicity of intrachain exchange interactions, as illustrated in Figure 1. In principle, such a ferrimagnetic AAF trimer chain seems to possess a 1/3 magnetization plateau; however, no plateau was observed up to the saturation magnetization.

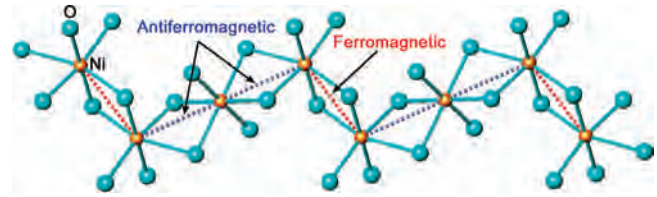

Figure 1. Illustration of the periodic magnetic exchange interactions in a NiO_6 chain of $ANi_3P_4O_{14}$ (A = Ca, Sr, Pb, Ba).[28]

(6) Maass, K.; Glaum, R.; Gruehn, R. *Z. Anorg. Allg. Chem.* **2002**, *628*, 1663–1672.
(7) El-Bali, B.; Boukhari, A.; Glaum, R.; Gerk, M.; Maass, K. *Z. Anorg. Allg. Chem.* **2000**, *626*, 2557–2562.
(8) El-Bali, B.; Boukhari, A.; Holt, E. M.; Aride, J. *J. Crystallogr. Spectrosc. Res.* **1993**, *23*, 1001.
(9) El-Bali, B.; Boukhari, A.; Aride, J.; Abraham, F. *J. Solid State Chem.* **1993**, *104*, 453–459.
(10) Hemon, A.; Courbion, G. *J. Solid State Chem.* **1990**, *85*, 164–168.
(11) (a) Bircsak, Z.; Harrison, W. T. A. *Acta Crystallogr., Sect. C* **1998**, *54*, 1554–1556. (b) El-Bali, B.; Bolte, M.; Boukhari, A.; Aride, J.; Taibe, M. *Acta Crystallogr., Sect. C* **1999**, *55*, 701–702.
(12) Belik, A. A.; Azuma, M.; Takano, M.; Lazoryak, B. I. *Chem. Mater.* **2004**, *16*, 4311–4318.
(13) Belik, A. A.; Azuma, M.; Matsuo, A.; Whangbo, M. H.; Koo, H. J.; Kikuchi, J.; Kaji, T.; Okubo, S.; Ohta, H.; Kindo, K.; Takano, M. *Inorg. Chem.* **2005**, *44*, 6632–6640.
(14) Belik, A. A.; Azuma, M.; Matsuo, A.; Kaji, T.; Okubo, S.; Ohta, H.; Kindo, K.; Takano, M. *Phys. Rev. B* **2006**, *73*, 024429.
(15) Boukhari, A.; Moqine, A.; Flandrois, S. *J. Solid State Chem.* **1990**, *87*, 251–256.
(16) Belik, A. A.; Azuma, M.; Takano, M. *Inorg. Chem.* **2003**, *42*, 8572–8578.
(17) Belik, A. A.; Azuma, M.; Takano, M. *J. Magn. Magn. Mater.* **2004**, *272*(276), 937–938.
(18) Moqine, A.; Boukhari, A.; Elammari, L.; Durand, J. *J. Solid State Chem.* **1993**, *107*, 368–372.
(19) Elmarzouki, A.; Boukhari, A.; Holt, E. M.; Berrada, A. *J. Alloys Compd.* **1995**, *227*, 125–130.
(20) Belik, A. A.; Azuma, M.; Takano, M. *Inorg. Chem.* **2005**, *44*, 7523–7529.
(21) (a) Riou, D.; Labbe, P.; Goreaud, M. *C. R. Acad. Sci.,Ser. II* **1988**, *307*, 903–907. (b) Riou, D.; Leligny, H.; Pham, C.; Labbe, P.; Raveau, B. *Acta Crystallogr., Sect. B* **1991**, *47*, 608–617.
(22) Belik, A. A.; Azuma, M.; Takano, M. *J. Solid State Chem.* **2004**, *177*, 883–888.
(23) Belik, A. A.; Uji, S.; Terashima, T.; Takayama-Muromachi, E. *J. Solid State Chem.* **2005**, *178*, 3461–3463.
(24) Faza, N.; Treutmann, W.; Babel, D. *Z. Anorg. Allg. Chem.* **2001**, *627*, 687–692.
(25) Belik, A. A.; Matsuo, A.; Azuma, M.; Kindo, K.; Takano, M. J. *Solid State Chem.* **2005**, *178*, 709–714.
(26) Matsuda, M.; Kakurai, K.; Belik, A. A.; Azuma, M.; Takano, M.; Fujita, M. *Phys. Rev. B* **2005**, *71*, 144411.
(27) Lii, K. H.; Shih, P. F.; Chen, T. M. *Inorg. Chem.* **1993**, *32*, 4373–4377.
(28) Hase, M.; Kitazawa, H.; Tsujii, N.; Ozawa, K.; Kohno, M.; Kido, G. *Phys. Rev. B* **2006**, *74*, 024430.
(29) Lemmens, P.; Güntherodt, G.; Gros, C. *Phys. Rep.* **2003**, *375*, 1.
(30) Haldane, F. D. M. *Phys. Rev. Lett.* **1983**, *50*, 1153–1156.
(31) Katsumata, K.; Hori, H.; Takeuchi, T.; Date, M.; Yamagishi, A.; Renard, J. P. *Phys. Rev. Lett.* **1989**, *63*, 86–88.
(32) Oshikawa, M.; Yamanaka, M.; Affleck, I. *Phys. Rev. Lett.* **1997**, *78*, 1984–1987.
(33) (a) Sakai, T.; Takahashi, M. *Phys. Rev. B* **1998**, *57*, R3201–R3204. (b) Kitazawa, A.; Okamoto, K. *Phys. Rev. B* **2000**, *62*, 940–945.
(34) (a) Narumi, Y.; Hagiwara, M.; Sato, R.; Kindo, K.; Nakano, H.; Takahashi, M. *Physica B* **1998**, *246*(247), 509–512. (b) Narumi, Y.; Kindo, K.; Hagiwara, M.; Nakano, H.; Kawaguchi, A.; Okunishi, K.; Kohno, M. *Phys. Rev. B* **2004**, *69*, 174405. (c) Hase, M.; Kohno, M.; Kitazawa, H.; Tsujii, N.; Suzuki, O.; Ozawa, K.; Kido, G.; Imai, M.; Hu, X. *Phys. Rev. B* **2006**, *73*, 104419.
(35) (a) Hida, K. *J. Phys. Soc. Jpn.* **1994**, *63*, 2359–2364. (b) Kitazawa, A.; Okamoto, K. *J. Phys.: Condens. Matter* **1999**, *11*, 9765–9774.
(36) Hagiwara, M.; Narumi, Y.; Minami, K.; Kindo, K.; Kitazawa, H.; Suzuki, H.; Tsujii, N.; Abe, H. *J. Phys. Soc. Jpn.* **2003**, *72*, 943–946.
(37) Inagaki, Y.; Kobayashi, A.; Asano, T.; Sakon, T.; Kitagawa, H.; Motokawa, M.; Ajiro, Y. *J. Phys. Soc. Jpn.* **2005**, *74*, 2683–2686.

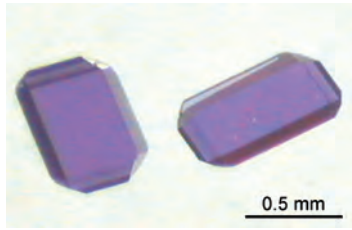

Figure 2. Morphology of single crystals of $BaCo_3P_4O_{14}$.

In this work, four phosphates, $BaCo_3P_4O_{14}$ (**1**), $SrCo_3P_4O_{14}$ (**2**), $BaMn_3P_4O_{14}$ (**3**), and $SrMn_3P_4O_{14}$ (**4**), have been synthesized by hydrothermal methods and analyzed by single-crystal X-ray diffraction; these species are isostructural with $ANi_3P_4O_{14}$ (A = Ca, Sr, Pb, Ba).[28] The MO_6 (M = Co, Mn) chains in **1**−**4** all conform to the same AAF trimer model as that in $ANi_3P_4O_{14}$ (A = Ca, Sr, Pb, Ba). Because of the antiferromagnetic interchain interactions, the net moments of ferrimagnetic MO_6 chains cancel each other perfectly in **3** to from a pure antiferromagnet and imperfectly in **1**, **2**, and **4** to form spin-canted antiferromagnets. Long-range orderings have een established at $T_{critical} \approx 8.2$ K for **1**, 6.5 K for **2**, and 2.6 K for both **3** and **4**. Interestingly, although they adopt the same ferrimagnetic chain model and show similar metamagnetisms in all analogues, only the Mn(II) system possesses 1/3 quantum magnetization plateaus at low temperature. This is also a rare example of the coexistence of classical and quantum natures (LRO and magnetization plateaus) at a finite temperature in 1D magnetic systems.

Experimental Section

Synthesis. All reagents were of analytical grade and were used as obtained from commercial sources without further purification. Single crystals of title compounds were synthesized under hydrothermal conditions at 200 °C. Typically, a ground mixture of 0.15 mmol of $A(CH_3COO)_2$ (A = Sr, Ba), 0.45 mmol of $M(CH_3COO)_2 \cdot 4H_2O$ (M = Co, Mn), and about 3 mL of concentrated H_3PO_4 (14.6 mol/L) were charged into a 50 mL Teflon reactor, which was then sealed in a stainless steel container. After they were heated at 200 °C for 5 days, the samples were extensively washed with hot water (80 °C). The products are transparent single crystals, as shown in Figure 2; these were purple for **1** and **2** and colorless for **3** and **4**. The purities for **1**, **2**, and **4** were confirmed by powder X-ray diffractions, and the yields, estimated on the basis of the transition metal, are about 80%. Compound **3** is difficult to obtain as a single phase, as it is always accompanied by the known phase $BaMnP_2O_7$. Therefore, dozens of single crystals of $BaMn_3P_4O_{14}$ were manually collected under a microscope and used for magnetic measurements. The other transition-metal resources, such as divalent metal chloride or nitrate, can also yield the same products. Among **1**−**4**, only $SrCo_3P_4O_{14}$ can also be synthesized by a high-temperature solid-state reaction: i.e. a ground mixture of $SrCO_3$, $Co(CH_3COO)_2 \cdot 4H_2O$, and $(NH_4)_2HPO_4$, in a molar ratio of 1:3:4, was first heated slowly to 600 °C in an alumina crucible. Then it was reground, pressed into a pellet, and reacted at 950 °C for 10 h.

Analyses. Representatively, a crystal of $BaCo_3P_4O_{14}$ with approximate dimensions 0.25 × 0.3 × 0.5 mm^3 was selected and used for single-crystal data collection at room temperature on a Bruker SMART X-ray diffractometer, equipped with an APEX-CCD area detector and graphite-monochromated Mo Kα radiation (λ = 0.710 73 Å) at 50 kV and 30 mA. A total of 4830 reflections were collected in the range $2.91° < \theta < 33.55°$, 1949 of which were independent and 1844 of which were observed ($I > 2\sigma$). The compound crystallizes in the monoclinic space group $P2_1/c$ (No. 14). An empirical absorption correction was applied on the basis of symmetry-equivalent reflections using the SADABS program.[38] The crystal structure was solved by using direct methods (SHELXS97)[39] and subsequent different Fourier analyses. The final refinements, carried on full-matrix least squares on F^2 using all unique data with anisotropic displacement parameters, led to R1 = 0.0206 and wR2 = 0.0593. The refined crystallographic parameters for $AM_3P_4O_{14}$ (A = Sr, Ba; M = Co, Mn) are presented in Table 1. For further details of structures, one may refer to the deposited data from the Fachinformationszentrum Karlsruhe, 76344 Eggenstein-Leopoldshafen, Germany (fax, (+49)7247-808-666; e-mail, crysdata@fiz-karlsruhe.de), on quoting the depository numbers CSD-417159, CSD-417450, CSD-417575 and CSD-417576.

Magnetic susceptibilities as a function of temperature were performed on a Quantum Design MPMS XL-7 (SQUID) system at an applied field of 500 Oe for **1** and 100 Oe for **2**−**4**, respectively. Crystals of $AM_3P_4O_{14}$ (A = Sr, Ba; M = Co, Mn) were ground and placed in a gelatin capsule fastened in a plastic straw for immersion into the SQUID system. The isothermal magnetization curves were measured up to 7 T for **1** and 5 T for **2**−**4**. Chemical analysis was carried out using ICP methods on an ESCALAB2000 analyzer. The measured atomic ratio for **1**, Ba:Co:P ≈ 1:2.72:3.75, reasonably agree with the proposed formula. Differential scanning calorimetric (DSC) measurements were carried out on a NETZSCH STA449C instrument at a heating rate of 10 °C/min under an argon atmosphere. Powder X-ray diffraction data were collected at room temperature on a Rigaku D/Max-2000 diffractometer (Cu Kα, λ = 1.5406 Å, 40 kV and 100 mA, graphite monochromator, scintillator detector, step scan 0.02°/3 s).

Results

Structure Description. The crystal structures of $AM_3P_4O_{14}$ (A = Sr, Ba; M = Co, Mn) are isostructural with $CaNi_3P_4O_{14}$,[27] crystallizing in the monoclinic space group $P2_1/c$ (No. 14). The asymmetric unit consists of 12 crystallographic independent atoms: M1 and Ba1 are located in the inversion center (2b and 2a sites); the rest of the atoms, including Co2, P1, P2, and seven O, are all located in general positions. The M1 and M2 atoms are both octahedrally coordinated by six oxygen atoms, while the P1 and P2 atoms are tetrahedrally coordinated. Figure 3 shows the overall structure of $BaCo_3P_4O_{14}$ as representative. The CoO_6 octahedra form zigzag chains running along the *b* axis, which are interconnected by P_2O_7 groups into a three-dimensional structure. The intrachain Co−Co distances are about 3.23 Å for Co1−Co2 and 3.29 Å for Co2−Co2, while the nearest interchain Co−Co distance is about 4.82 Å via an O−P−O linkage.

The bond valence sums (BVS) calculation indicates that all the metal ions are normally divalent (BVS = 1.988 (Co1) and 1.865 (Co2) for **1**, 1.994 (Co1) and 1.912 (Co2) for **2**,

(38) Sheldrick, G. M. *SADABS, Siemens Area Detector Absorption Correction Program*; University of Göttingen: Göttingen, Germany, 1994.
(39) Sheldrick, G. M. *SHELXS 97, Program for the Solution of Crystal Structures*; University of Göttingen, Göttingen, Germany, 1997. *SHELXL 97, Program for the Refinement of Crystal Structures*; University of Göttingen, Göttingen, Germany, 1997.

Table 1. Crystallographic Parameters and Refinement Results for $AM_3P_4O_{14}$ (A = Sr, Ba; M = Co, Mn)

	$BaCo_3P_4O_{14}$	$BaMn_3P_4O_{14}$	$SrCo_3P_4O_{14}$	$SrMn_3P_4O_{14}$
CSD no.	417159	417450	417575	417576
formula wt	662.00	650.03	612.29	600.32
temp (K)		293		
radiation λ (Å)		0.710 73		
cryst size (mm)	0.25 × 0.3 × 0.5	0.25 × 0.3 × 0.5	0.2 × 0.25 × 0.4	0.2 × 0.25 × 0.4
color	purple	colorless	purple	colorless
space group		$P2_1/c$		
a (Å)	7.5749(15)	7.7783(16)	7.4690(15)	7.6706(15)
b (Å)	7.8349(16)	7.9207(16)	7.7088(15)	7.7950(16)
c (Å)	9.6343(19)	9.784(2)	9.4955(19)	9.6444(19)
β (deg)	112.70(3)	112.49(3)	111.97(3)	111.75(3)
V (Å^3)	527.5(2)	557.0(2)	507.0(2)	535.6(2)
Z		2		
ρ_{calcd} (g/cm^3)	4.168	3.876	4.011	3.722
μ(Mo Kα) (mm^{-1})	9.014	7.472	10.779	9.094
no. of rflns collected	4830	5033	4695	4930
no. of indep rflns	1949	2033	1875	2002
$I > 2\sigma(I)$	1844	2004	1782	1909
θ range (deg)	2.91–33.55	2.83–33.33	2.94–33.44	2.86–33.40
GOF	1.000	1.000	1.000	1.000
R1 ($I > 2\sigma(I)$)	0.0206	0.0530	0.0348	0.0215
wR2 (all data)	0.0593	0.1644	0.1043	0.0645

2.112 (Mn1) and 1.970 (Mn2) for **3**, and 2.114 (Mn1) and 2.015 (Mn2) for **4**). The thermal stabilities of **1**−**4** have been investigated by DSC measurements (see Figure S1 in the Supporting Information). On heating, **1** and **2** retain stable up to their melting points (1039 and 1113 °C), while **4** starts to decompose into two known phosphates ($Mn_2P_2O_7$[40] and $SrMn_2P_2O_7$[41]) above 700 °C (see Figure S2 in the Supporting Information); the DSC curve of **3** is similar to that of **4**, suggesting a possible similar decomposition at high temperature.

Magnetic Properties. Figure 4 gives the magnetic susceptibilities (χ) measured in the temperature range 2–300 K at an applied field of 500 Oe for **1** and 100 Oe for **2**−**4**, respectively, using polycrystalline samples. In the high-temperature region (above 30 K), the ZFC and FC curves are almost identical and follow the Curie–Weiss law (Figure 4b). The fitted parameters together with the measured effective magnetic moments ($\mu_{eff} = (8C)^{1/2}$) are given in Table 2. These μ_{eff} values are typical for Co^{2+} (d^7, $S = 3/2$)

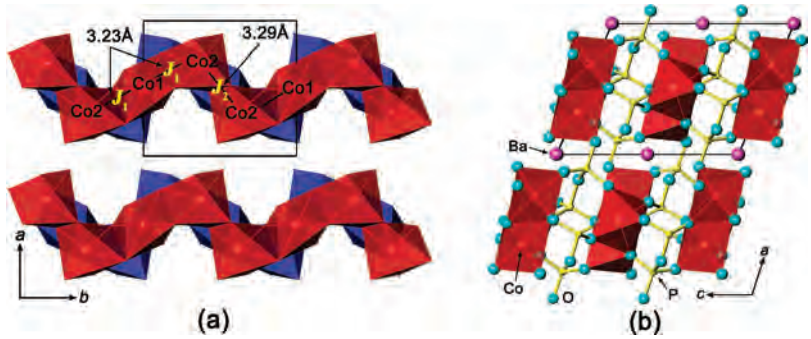

Figure 3. (a) CoO_6 chains in $BaCo_3P_4O_{14}$ viewed along the c axis. P_2O_7 groups are omitted for clarity. (b) Projection of the complete structure along the b axis.

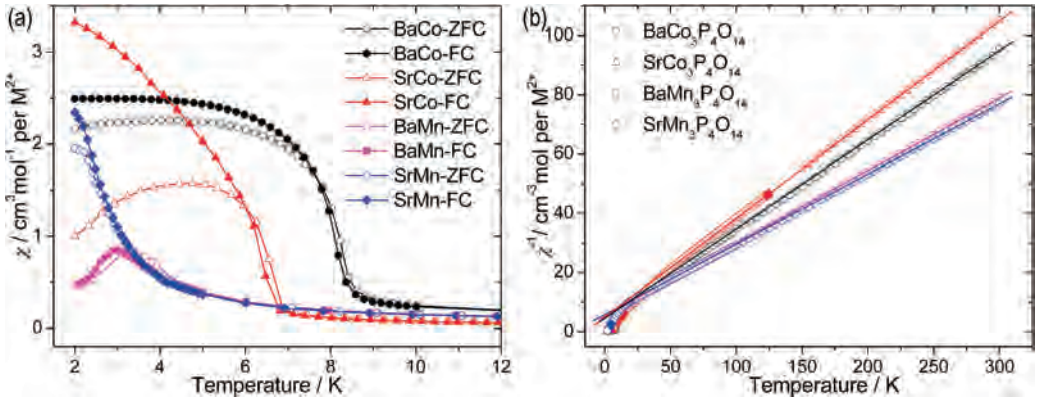

Figure 4. (a) Magnetic susceptibilities (χ is presented per M^{2+} ion) in the low-temperature region for **1** (at 500 Oe) and **2**−**4** (at 100 Oe) under both ZFC and FC conditions. The curves of **2** are triply divided. (b) Curie–Weiss law fit of the reciprocal paramagnetic susceptibilities χ^{-1}.

Table 2. Fitted parameters for $\chi(T)$ using the Curie–Weiss lLaw (above 30 K) and the Ordering Temperatures $T_{critical}$

	Θ (K)	C (cm^3 mol^{-1} K/M^{2+})	μ_{eff} (μ_B)	g	$T_{critical}$ (K)
$BaCo_3P_4O_{14}$	−13.3	2.82	4.75	2.45	8.2
$SrCo_3P_4O_{14}$	−15.6	3.01	4.91	2.53	6.5
$BaMn_3P_4O_{14}$	−19.8	4.06	5.70	1.93	2.6
$SrMn_3P_4O_{14}$	−22.3	4.18	5.78	1.95	2.6

and Mn^{2+} (d^5, $S = 5/2$).[42] The g factors, which are calculated from the Curie constants ($8C = g^2S(S + 1)$), are 2.45 for **1** and 2.53 for **2**; large g values are common for the Co^{2+} systems, due to the strong spin–orbital coupling and the large anisotropy.

On the basis of the structure−magnetism relation, the magnetic behaviors of **1**−**4** can all be understood by applying a ferrimagnetic chain model and the chains are antiferromagnetically coupled to be either a pure or a spin-canted antiferromagnet. The magnetic model will be explained in the Discussion. When these compounds were cooled, the χT curves of **1**−**4** first decreased smoothly to a minimum, followed by a sharp increase (see Figure 5). The decrease indicates the dominant magnetic interactions in **1**−**4** are antiferromagnetic, consistent with the negative Weiss temperatures (Θ) for all four compounds. The subsequent increase of χT indicates that there exists some kind of ferromagnetic component which is in fact corresponding to the net magnetic moments of ferrimagnetic chains. With further cooling, **1**−**4** behave differently. As shown in Figure 4a and 5a, the ZFC and FC curves diverge for **1**, **2**, and **4**, implying the presence of the long-range ordered state with spontaneous magnetism. Since metamagnetic behaviors were detected in the isothermal magnetization measurements, which imply that the interchain interactions are antiferromagnetic for all four compounds, the spontaneous magnetism therefore derives from the spin-canted antiferromagnetism, which leads to the imperfect cancelation of the net moments of ferrimagnetic chains. Compound **3**, on the other hand, does not show such an obvious divergence but has a maximum at about 3 K in $\chi(T)$, indicating that the net moments cancel each other perfectly and an ordered pure antiferromagnetic state is established. The critical temperatures ($T_{critical}$) for the long-range ordering, estimated form the d(χT)/d(T) curves (see Figure S3 in the Supporting Information), are also given in Table 2.

Figure 6 shows the isothermal magnetization curves at 2 K for **1**−**3** and at 1.9 K for **4**. The spontaneous magnetic components for **1** and **2** can be clearly seen from the hysteresis loops in the magnetization curves shown in parts a and b of Figure 6, with coercive forces (H_c) and remanence (M_R) of about 1500 Oe and 0.172 μ_B for **1** and 110 Oe and 0.175 μ_B for **2**. In addition, a field-induced spin-flop-like transition occurs in **1** and **2**, and the critical fields are 23 kOe for **1** and 4 kOe for **2**, estimated from the dM/dH curves, which are shown as the right-hand insets of parts a and b of Figure 6. It is noted that there exist well-defined magnetization jumps near $H = 0$ Oe in the dM/dH vs H curve for **2**, which were suggested to be caused by abrupt changes in the domain structure: e.g., abrupt domain-wall motion.[43]

From the $M(H)$ curve, **3** is a typical metamagnet: from antiferromagnetic ground state to ferromagnetic excited state. The critical field is 3 kOe, estimated from the dM/dH plot shown in the right-hand inset of Figure 6c. For **4**, no hysteresis loop is observed even at 1.9 K, although the $\chi(T)$ plots shows a divergence between ZFC and FC curves, possibly because 1.9 K is not lower than the long-range ordering temperature. It is common that the coercive field and the remanent moment will increase with decreasing temperature. The dM/dH plot for **4** is very similar to that for **2**, including a jump at $H = 0$ and two side peaks at $H \approx \pm 0.7$ kOe, which indicates that a spin-flop-like phase transition happens at $H \approx 0.7$ kOe. Similar phase transitions were also observed in $A_3Cu_3(PO_4)_4$ (A = Sr, Pb)[25] at an even lower field of 0.3 kOe at 0.08 K. Interestingly, the magnetizations show a quick saturation at 1.72 μ_B for **3** and at 1.71 μ_B for **4**, very close to 1/3 of the saturation (5 μ_B for Mn^{2+}, $S = 5/2$). It is an evident 1/3 magnetization plateau. A higher magnetic field (>5 T) is needed to make a jump to the fully magnetized state. This is an interesting phenomenon, and we have measured the magnetizations around the long-range ordering temperature (2.6 K). As shown in the left-hand insets of parts c and d of Figure 6, the 1/3 plateaus or tendency for plateaus can be also observed above 2.6 K, which points to the quantum nature of these magnetization plateaus.

In summary, the magnetic properties of **1**−**4** can be summarized as follows: all four compounds have ferrimagnetic MO_6 chains; these chains are antiferromagnetically coupled by weak interchain interactions with long-range orderings to form a pure antiferromagnet at 2.6 K for **3** or spin-canted antiferromagnets at 8.2 K for **1**, 6.5 K for **2**, and 2.6 K for **4**, respectively; field-induced spin-flop-like transitions occur at $H_c \approx 25$ kOe for **1**, 4 kOe for **2**, 3 kOe for **3**, and 0.7 kOe for **4**; both **3** and **4** show a 1/3 quantum magnetization plateau.

Discussion

$AM_3P_4O_{14}$ (A = Ba, Sr; M = Ni, Co, Mn) are all isostructural; thus, they provide an interesting model system to study quasi-one-dimensional magnetic interactions. Two superexchange interactions are expected within the chain, corresponding to two distinct Co−Co distances, i.e., Co1−Co2 = 3.23 Å and Co2−Co2 = 3.29 Å; the magnetic interaction constants are respectively J_1 and J_2 (see Figure 3a). One expects comparatively smaller interchain interactions because the nearest interchain Co−Co distance is about 4.82 Å (via a Co−O−P−O−Co pathway). Therefore, at the first approximation, $AM_3P_4O_{14}$ (A = Ba, Sr; M = Ni, Co, Mn) can be considered as trimeric magnetic ($J_1-J_1-J_2$) chain com-

(40) Stefanidis, T.; Nord, A. G. *Acta Crystallogr., Sect. C* **1984**, *40*, 1995–1999.
(41) Maass, K.; Glaum, R. *Acta Crystallogr., Sect. C* **2000**, *56*, 404–406.
(42) (a) Mabbs, F. E.; Machin, D. J. *Magnetism and Transition Metal Complexes*; Chapman and Hall: London, 1973. (b) Figgis, B. N.; Hitchman, M. A. *Ligand Field Theory and Its Applications*; Wiley-VCH: New York; 2000.
(43) Adams, R. D.; Layland, R.; Payen, C.; Datta, T. *Inorg. Chem.* **1996**, *35*, 3492–3497.

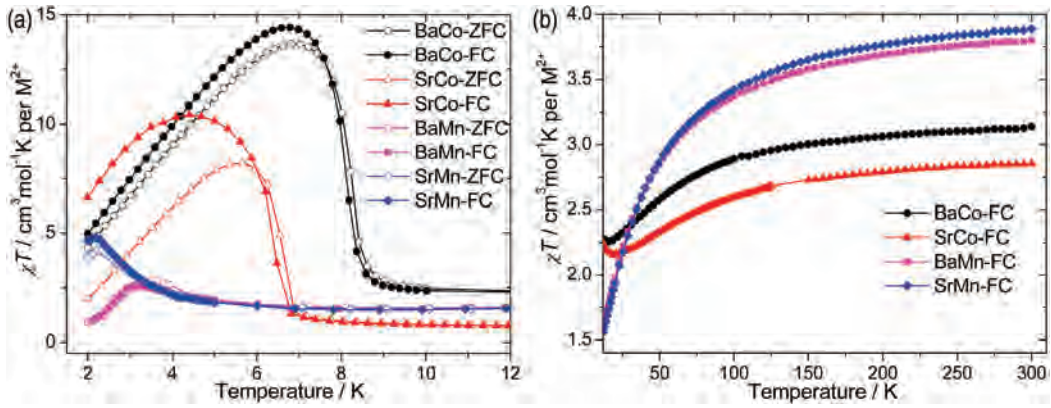

Figure 5. Temperature dependence of the χT products for **1**−**4** in the ranges (a) 2–12 K and (b) 12–300 K. Note that the curves of **2** in the low-temperature region are triply divided.

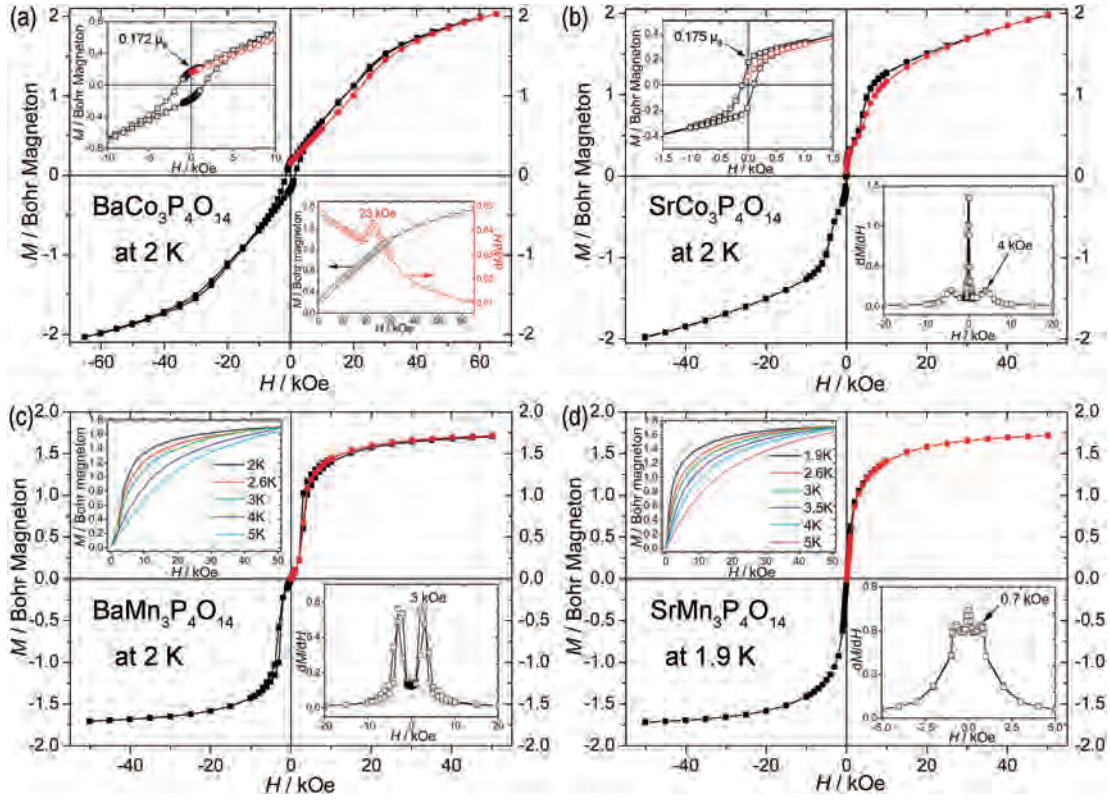

Figure 6. Field dependence of magnetization plots. The magnetization is presented per M^{2+} ion. The red curves represent the initial magnetization processes for each compound. The insets are the enlargement of low-field magnetic hysteresis loops, dM/dH curves, or M vs H at various temperatures.

pounds. It should be kept in mind that this magnetic model is not ideal but quasi-one-dimensional, because all of the species have a long-range ordering at finite temperatures.

Hase et al.[28] interpreted the magnetic properties of $ANi_3P_4O_{14}$ (A = Ca, Sr, Pb, Ba) with an antiferromagnetic−antiferromagnetic−ferromagnetic trimerized chain model. Other possible models, such as FFF, AAA, and FFA, were also considered but were ruled out according to the experimental observations. The interchain interaction is predominantly antiferromagnetic; however, due to the single-ion anisotropy of Ni^{2+} spins, the magnetic moments of the ferrimagnetic chains are not perfectly canceled and thus the system is a spin-canted antiferromagnet with a small spontaneous field. The quantum Monte Carlo simulation based on the AAF model reproduces the observed high-field magnetization reasonably well.

Table 3. Spin Orientations of the Four Possible Trimer Models and the Relevant Consequences

model	spin orientation	chain net moment	Θ
AAA	↑↓↑↓↑↓↑↓↑↓	no	negative
FFA	↑↑↓↓↑↑↓↓	no	positive or negative
FFF	↑↑↑↑↑↑↑↑↑↑	yes	positive
AAF	↑↓↑↓↑↓↑↓	yes	positive or negative

Since **1**–**4** are isostructural with $ANi_3P_4O_{14}$ (A = Ca, Sr, Pb, Ba), it is most appropriate to apply the same AAF trimer model. However, the other three possible trimer models should also be reconsidered for the title compounds in this case. Table 3 gives the spin orientations in all four possible trimer chain models and the relevant consequences, where "chain net moment" refers to whether there is a net magnetic moment within a single chain. Note that a very important result can be directly gathered from Hase's work:[28] there is

no net magnetic moment within a single chain in the AAA and FFA models because of the limitations of the structural symmetry.

The FFF model can be first ruled out because **1**−**4** all have negative Θ values. When the systems were cooled, the χT values of **1**−**4** first decreased, followed by an anomalous upturn in the low-temperature regions, which means they all have a net magnetic moment within a single chain, and in fact the chain net moments canceled each other perfectly or imperfectly to form pure (for **3**) or spin-canted antiferromagnets (for **1**, **2**, and **4**). Accordingly, it is clear that the AAF model is the only suitable model to interpret the magnetic behaviors of the compounds **1**−**4**.

$AM_3P_4O_{14}$ (A = Ba, Sr; M = Ni, Co, Mn) all have the same AAF ferrimagnetic chain model. The 1/3 magnetization plateaus show up both below and above the ordering temperatures in **3** and **4**, which means that the plateaus are not the consequence of long-range orderings; these plateaus are also insensitive to the external field (we use polycrystalline samples for measurements). All these facts point to the quantum nature of these magnetization plateaus. Despite the qualitatively identical spin models, the 1/3 plateaus only appear in Mn analogues, not in Ni and Co analogues. Thus, it is intriguing to note the specific requirements of the appearance of quantum magnetization plateaus in AAF trimerized chain compounds.

It is apparent that the quantum nature of these magnetization plateaus demands good low dimensionality at first. The ordering temperature, which reflects 1D characteristics, decrease from the Ni analogues (∼15 K) to the Co analogues (∼8.2 K) and to the Mn analogues (∼2.6 K). This then does imply an increase of the 1D characteristics from the Ni to the Mn systems. On the other hand, from pioneering work, we noted that the magnitude of the ratio J_F/J_{AF} should be small for the appearance of the magnetization plateau in ferromagnetic−antiferromagnetic mixed chains, such as the FFA chain.[35] However, the AAF model has not yet been extensively studied, probably due to the absence of model compounds. As an approximate case of the AAF model, $Ca_3Cu_3(PO_4)_4$ has $S_{total} = 1/2$ trimer clusters which are linearly interconnected by very weak FM interactions. Indeed, a 1/3 magnetization plateau is detected above 12 T at 1.6 K.[25] Therefore, one could expect a 1/3 magnetization plateau with a visible width derived from a combination of strong AF and weak FM intrachain interactions in the AAF model. In our system, the values of Θ, which are in fact the algebraic sums of all the exchange interactions, are increasingly negative on going from Ni to Mn systems.[44] After making a deduction of the negative components of antiferromagnetic interchain interactions, which are actually increasingly smaller on going from Ni to Mn systems, as reflected by the ordering temperatures, we can conclude that the AF intrachain interactions of Mn analogues are the most dominant in all analogues. Therefore, it is reasonable that the magnetization plateau in the Ni system is absent, because of the loss of the 1D characteristics ($T_c \approx 15$ K) and the weak AF intrachain (roughly 1/10 of the ferromagnetic exchange) interactions, which may be the same for the Co system. Comparatively, **3** and **4** have the best 1D characteristics and the strongest AF intrachain interactions; consequently, 1/3 magnetization plateaus are detected only in $BaMn_3P_4O_{14}$ and $SrMn_3P_4O_{14}$.

(44) In ref 28, the absolute values of Θ in $ANi_3P_4O_{14}$ (A = Ca, Sr, Pb, Ba) were not directly reported but only a rough estimate (less than a few degrees Kelvin) was given. In this work,we obtained the single-crystal samples of both $BaNi_3P_4O_{14}$ and $SrNi_3P_4O_{14}$ by hydrothermal methods and measured their magnetic susceptibilities. The Curie−Weiss fit using the data above 40 K generated Θ = −3.2 K for $BaNi_3P_4O_{14}$ and Θ = −1.8 K for $SrNi_3P_4O_{14}$.

Conclusions

In conclusion, we synthesized the four new phosphates $AM_3P_4O_{14}$ (A = Sr, Ba; M = Co, Mn) hydrothermally and determined their crystal structures by single-crystal X-ray diffraction. They are isostructural with $ANi_3P_4O_{14}$ (A = Ca, Sr, Pb, Ba), and we interpreted their magnetic behaviors by applying the same AAF trimer chain model as in Ni analogues. Therefore, they contain ferromagnetic chains composed of MO_6 octahedra and all have a long-range magnetic ordering (spin-canted antiferromagnetic for **1**, **2**, and **4** and pure antiferromagnetic for **3**) at low temperature and a field-induced magnetic phase transition due to weak interchain AF interactions. Most interestingly, only $BaMn_3P_4O_{14}$ and $SrMn_3P_4O_{14}$ have 1/3 quantum magnetization plateaus. We have compared the differences between among $AM_3P_4O_{14}$ species (A = Sr, Ba, M = Ni, Co, Mn) and made a qualitative speculation that the appearance of a quantum magnetization plateau in an AAF trimer chain requires both good 1D characteristics and the strong AF intrachain interactions. Further quantitative analyses require the efforts of physicists. However, the specific spin configurations remain unclear, and to solve this matter, neutron diffraction experiments are needed.

Acknowledgment. This work was supported by the Nature Science Foundation of China, under Contract Nos. 20221101 and 20771008.

Note Added after ASAP Publication. This article was released ASAP on March 12, 2008, with the right hand insets of parts c and d in Figure 6 reversed. The correct version was posted on March 31, 2008.

Supporting Information Available: CIF files giving crystal data and figures giving DSC curves, XRD patterns of samples treated at different temperatures, and d(χT)/d(T) curves. This material is available free of charge via the Internet at http://pubs.acs.org.

IC702346E